A prototype coarse pointing mechanism for laser communication

Eric D. Miller*[a], Michael DeSpenza[b], Ilya Gavrilyuk[b], Graham Nelson[b], Brent Erickson[b], Britney Edwards[b], Ethan Davis[b], Tony Truscott[b]
[a]Facebook, Inc., 1 Hacker Way, Menlo Park, CA, USA 94025-1456;
[b]Quartus Engineering, Inc., 9689 Towne Center Dr., San Diego, CA, USA 92121-1964

ABSTRACT

Laser communication systems promise orders-of-magnitude improvement in data throughput per unit SWaP (size, weight and power) compared to conventional RF systems. However, in order for lasercom to make sense economically as part of a worldwide connectivity solution, the cost per terminal still needs to be significantly reduced.

In this paper, we describe a coarse pointing mechanism that has been designed with an emphasis on simplicity, making use of conventional materials and commercial off-the-shelf components wherever possible. An overview of the design architecture and trades is presented, along with various results and practical lessons learned during prototype integration and test.

Keywords: optical communication, free-space optics, lasercom, pointing, PAT, mechanism, flex wrap, torque testing

1. INTRODUCTION

Myriad books and papers have been published promoting the advantages of laser communication (lasercom) over radio frequency (RF) systems[1-3]. Indeed, several examples of successful technology demonstrations can be found spanning back multiple decades[4-10]. More recently, a growing wave of industry groups have been exploring lasercom as a component of worldwide broadband networks[11-17].

In order for lasercom to make sense economically, the size, weight, power, and especially cost (SWaP+C) of the terminals must be reduced. With this in mind, Facebook is investigating various lasercom-related technologies that push the state-of-the-art in terms of throughput per SWaP+C and other metrics. In this paper, we present one ongoing effort focused on developing a Coarse Pointing Assembly (CPA) capable of providing precision line-of-sight (LOS) articulation over a near-hemispherical field of regard (FOR). The generic design form of this CPA does resemble that presented in other papers[18,19], however in our system we have placed a significant emphasis on meeting our requirements with the simplest design implementation possible, using mainly commercial off-the-shelf (COTS) components, and striving to establish a clear path forward to more-economical, larger-scale production in the future.

Some of the main design drivers, along with a photograph of the prototype assembly, are shown in Figure 1.

Main Design Drivers:

- Clear aperture > 60 mm
- Near-hemispherical FOR (>330° in azimuth and elevation)
- Open-loop pointing accuracy < 500 µrad
- Peak slew rate > 10°/sec
- Wavefront distortion < 20 nm RMS
- Mass < 4 kg
- Power consumption < 10 W
- Harsh non-operational random vibration
- Wide temperature range
- Non-negligible radiation environment

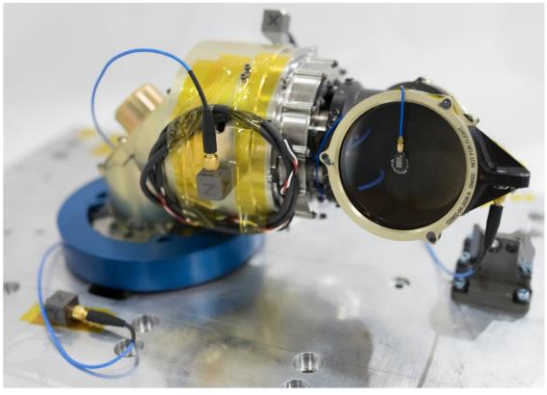

Figure 1. Prototype CPA and main design drivers

*ericmi@fb.com

In Section 2 we present an overview of the design architecture and trades, followed by detailed description of the drive elements, optics, launch lock assembly, flex print circuits, and thermal management features. Section 3 describes some of the vibration, thermal, and optical performance analyses that were used to help inform the initial design development. Section 4 then describes some of the integration and test activities that were performed using prototype hardware. Finally, Section 5 summarizes the results and lessons learned, and proposes a brief list of ideas that we believe are worthy of future investigation.

2. DESIGN

2.1 CPA design overview

At a high level, the CPA design resembles a gimbaled periscope, where two flat mirrors direct the optical line of sight through a hollow tube, and two orthogonal axes of rotation provide wide-angle steering capability. This design form is sometimes referred to as a *coelostat*[20].

The major subassemblies in this CPA design are the drive assemblies (quantity 2), the elbow assemblies (quantity 2), the flex wrap assemblies (quantity 2), and the launch lock assembly (quantity 1). The drives assemblies provide smooth, precise rotary motion, the elbow assemblies provide mounting structure for the fold mirrors, the flex wraps carry the motor and resolver electrical signals across the rotating interfaces, and the launch lock provides supplemental structural support to protect the bearings and prevent motion during exposure to high random vibration environments. Each of these assemblies will be described in more detail in the following sections. An exploded view of the CPA is shown in Figure 2.

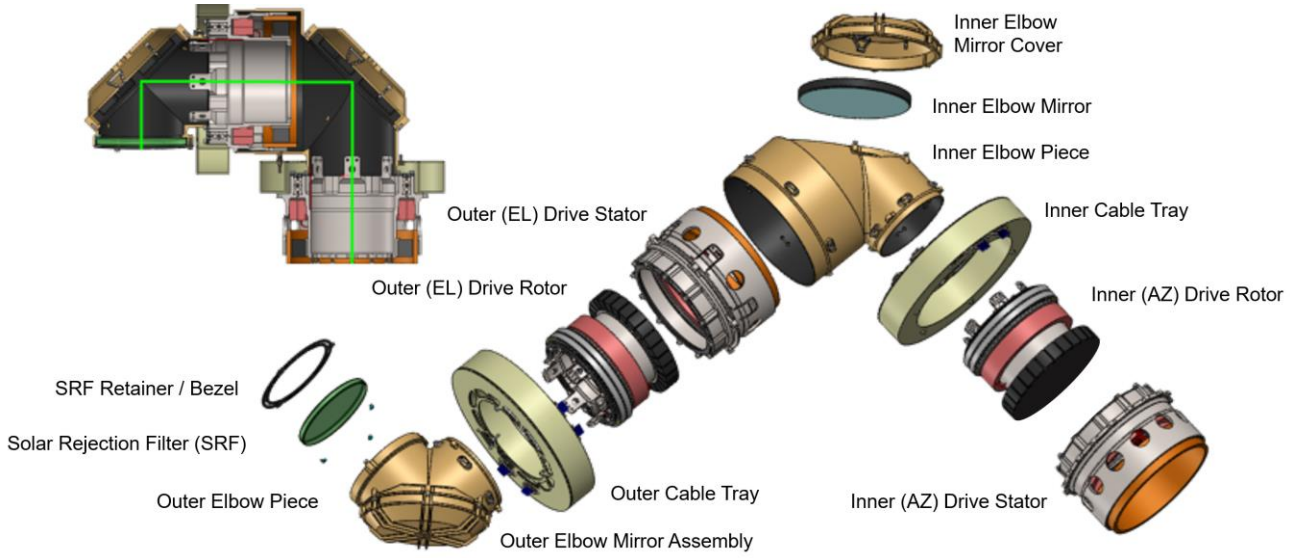

Figure 2. CPA exploded view

2.2 Drive assembly design

The primary function of the drive assemblies is to provide smooth, accurate rotary motion, with built-in sensing devices to support closed-loop position control. Figure 3 provides a section view of the azimuth and elevation drive assemblies.

The bearing configuration was carefully selected to ensure adequate structural stiffness, minimal runout, and minimal drag torque. A back-to-back duplex pair of angular contact bearings was used on each axis, with silicon nitride ceramic load balls, toroidal PTFE spacers, and 440C stainless steel races manufactured to ABEC 7 tolerances.

Just as important as the bearing construction was the lubricant selection. Due to the boundary lubrication regime of the slow-moving CPA, a non-PFPE lubricant was desired. (The very reaction that enables PFPE-based lubricants such as Braycote 601EF to function in boundary lubrication conditions also hastens the chemical decomposition and eventual bearing failure.[21]) The best-performing and most-common non-PFPE lubricant choice for boundary lubrication applications is multiply alkylated cyclopentane (MACs), a synthetic hydrocarbon commercially available as Pennzane in

various formulations of oil and grease. Pennzane-based lubricants have demonstrated longer lubricant lifetimes and more-gradual progressions to failure over PFPE-based and other lubricants typically employed for space. For our prototype CPA, Nye Rheolube 2000 was selected for its performance, heritage, and availability. The Rheolube 2000 series products are specifically developed for precision instruments and bearings in aerospace and vacuum application. The grease consists of MAC thickened with a sodium complex soap, and formulated with anti-wear, anti-oxidant, anti-corrosion, and extreme pressure additives to improve performance. The downside to MAC-based lubricants is an increased viscosity at low temperature, but heaters solve this problem, and are also needed to maintain adequate temperature gradient across the bearings anyway. Nye Bar barrier film was also used to prevent migration of the lubricant onto the optical surfaces.

The motors are commercially available, three-phase, direct-drive slotless brushless DC motors, which when sinusoidally commutated provide the smoothest actuation possible. Since these motors provide zero un-powered holding torque, it was initially thought that a separate brake or "park-stop" mechanism would be necessary. However, upon further investigation it was determined that the minimum drag torque in the bearings (though intentionally low) would always be enough to resist any reaction torques caused by host platform motion. Therefore, a dedicated park-stop motion was not necessary.

For shaft position measurement, commercially available absolute resolvers were used. These resolvers feature dual-speed windings (1x and 16x) for improved precision over a full 360-degree rotation. Alternative position sensor options such as optical encoders were considered, however the leading optical encoders had not been qualified for our environment, and others that were qualified had very high cost and lead times. Initially it was thought that using resolvers would incur a significant accuracy hit compared to optical encoders. However, we were able to calibrate the resolver measurements from an uncalibrated accuracy of ± 200 µrad down to a calibrated accuracy of ± 20 µrad. (More on this calibration process in Section 4.5.)

The motors, resolvers, and bearings are all integrated into a titanium 6AL-4V shaft & housing. Titanium was selected for its close CTE match with the bearing races and motor and resolver back iron. A Tiodize Type II surface treatment was applied to prevent wear and minimize FOD generation. While titanium does provide a significant weight savings over other CTE-matching materials (such as steel), further weight savings could be achieved using advanced materials such as AlBeMet. However, for our system, the high manufacturing cost of AlBeMet was not justified by the amount of weight savings, so we decided to use titanium for now.

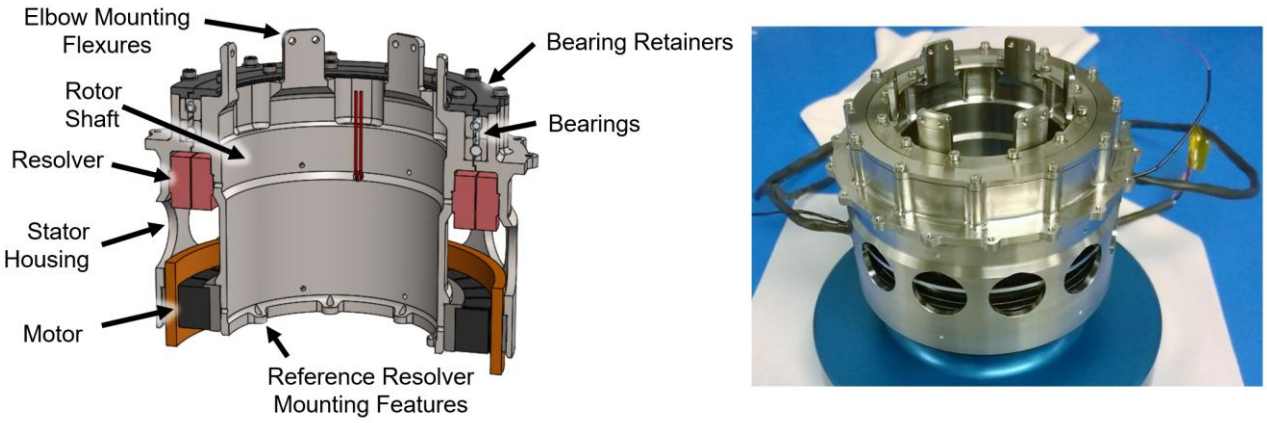

Figure 3. Drive assembly CAD & prototype assembly

2.3 Elbow assembly design

The elbow assemblies each include a light-weighted flat mirror, suspended on a trio of bipod flexures, mounted to a right-angle tube section. The inner elbow provides structural support for the elevation drive and outer elbow assemblies, whereas the outer elbow provides the second right angle turn, and also integrates a solar rejection filter at the output.

Although the mirrors are small and flat, the initial requirements of <10 nm RMS surface figure and <2nm RMS surface roughness presented a reasonable manufacturing challenge. An aluminum substrate was initially considered for its low

cost and CTE match to the mating elbows. Standard alloys (6061) and processes (single point diamond turning) were considered along with advanced RSP alloys and processes including AlumiPlate, Chemical Mechanical Polishing (CMP), ELCAN's VQ, and more. After consulting with multiple vendors, the bare aluminum option seemed riskier than other options such as AlBeMet, beryllium, silicon carbide, Zerodur, and more. Several vendors suggested nickel-plated aluminum, which we wanted to avoid for concerns of bimetallic bending/distortion over temperature[22]. In the end, a Zerodur substrate with titanium mounting flexures met all of the performance and environment requirements levied on the prototype CPA, with a satisfactory cost and lead-time. Protected gold was used for its high reflectance in the NIR spectrum.

Because of the mismatch in CTE of the Zerodur mirrors and aluminum elbows, a compliant interface was required to maintain mirror figure across environments. Titanium bipod flexures were optimized to survive vibration loads while minimizing thermal distortion on the mirror. The low thermal conductivity helps to isolate the Zerodur mirror from neighboring components, thereby minimizing thermal gradients and distortion within the mirror itself. The titanium flexures are bonded to the back of the Zerodur mirror using a "saddle" like configuration, again to minimize mirror distortion during operation. In order to minimize mirror distortion due to high-CTE of suitable adhesive, bond-line thickness was precisely controlled. To ensure the bond lines are of appropriate size without imposing excessive tolerances on the mirror and flexure vendors, each flexure's bonding "saddle" is machined to match the mating rib of the mirror. This match machining method, analogous to the bearing retainers, requires additional inspection and processing steps, but ensures desired performance. Tooling and in-situ inspections ensure the position and alignment of the flexure with respect to the mirrors during bonding.

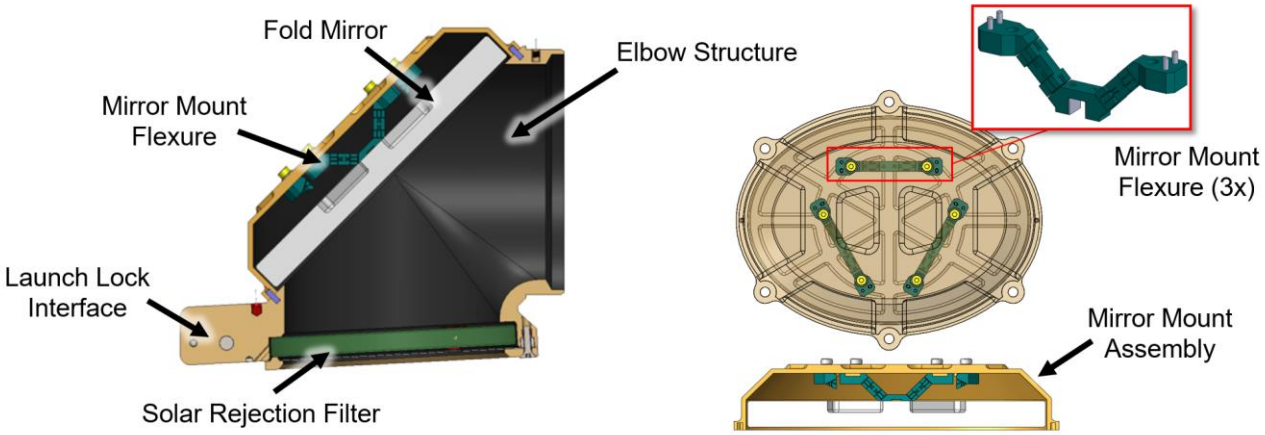

Figure 4. Elbow assembly design

2.4 Flex wrap assembly design

There are several electrical signals (e.g., motor currents, resolver inputs & outputs, and heater & thermistor signals), which must be transferred across the rotating drive assembly joints. Our approach for accommodating these interfaces is to use flexible printed circuits (FPCs), arranged in a rolling, "horizontal gooseneck" configuration[23]. These FPCs consist of thin layers of copper, sandwiched between insulative layers of adhesive and Kapton. The two ends of the FPC are reinforced with conventional PCB stiffeners, which are connectorized and used for mounting. Figure 5 shows how the FPCs are installed in the system. In order to qualify our FPC design against fatigue failure, lifetime testing was performed using an automated test setup. More information on the test method and the detailed design configurations we tested is provided in Section 4.4.

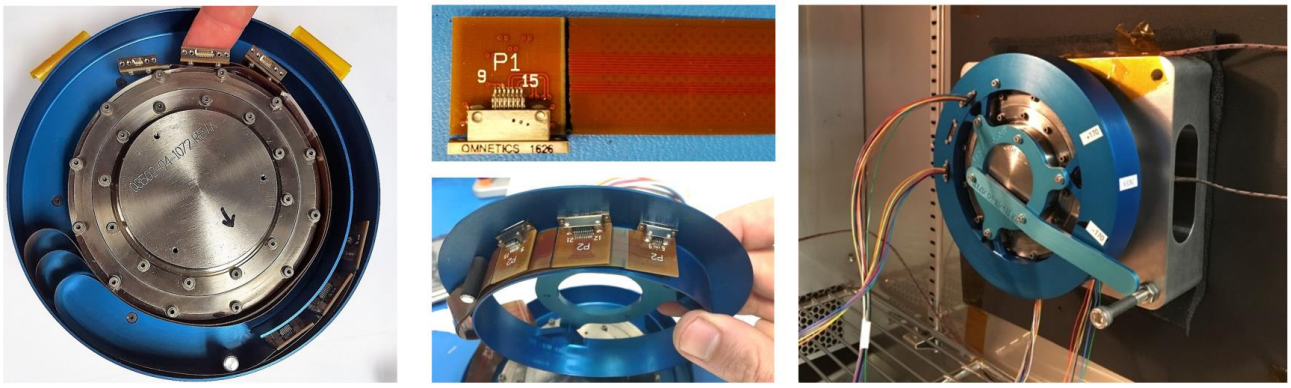

Figure 5. Flex wrap design & installation photos. (Far right = flex circuit lifetime test rig.)

2.5 Launch lock assembly design

A launch lock assembly was needed for two reasons: (1) to off-load the bearings to protect against extreme loading or gapping, and (2) to prevent free rotation – both reasons relevant primarily during exposure to harsh non-operational vibration loads. Gapping is the phenomena whereby external loads and moments are sufficient to overcome the applied bearing preload, thereby offload some of the balls in the bearing and producing a small clearance between said balls and the races. While gapping is not explicitly prohibited by design manuals and recommendations, it is generally understood to be undesirable, especially when due to vibration[24]. Gapping presents a dynamic non-linearity in the bearing stiffness and the possibility of damage to lubricant, ball and races occurs with load reduction or reversal[25].

When ready for deployment, post vibration environments, the launch lock assembly releases the CPA for operation. The desire was to create a lightweight, robust, and rigid launch lock assembly. The risk of debris from a friction interface reacting vibration loads motivated the use of a cup and cone to carry shear forces (i.e. normal to the Frangibolt axis). The design of the cup and cone, surface finishes, tolerances, and inspection process ensure that the Frangibolt will always break when activated. Furthermore, this design allows the CPA to return to the locked position, utilizing the cup and cone as a locating reference for various calibration activities.

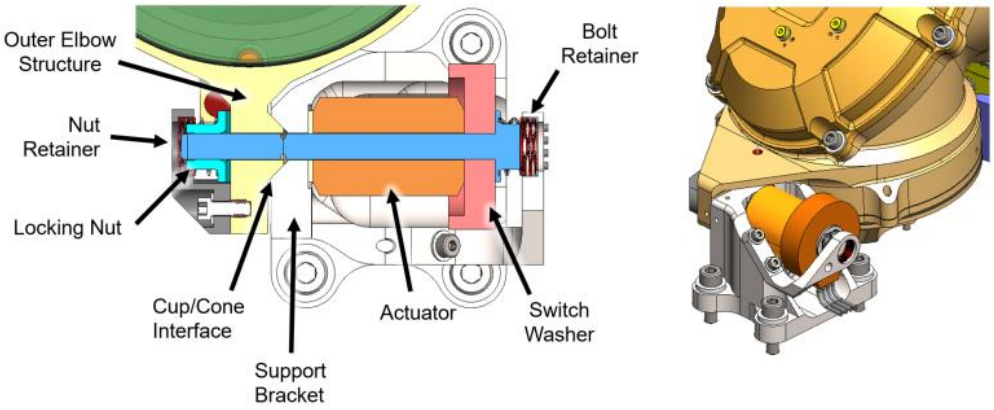

Figure 6. Launch lock assembly design

2.6 Other design features

The drag torque in the bearings is sensitive in two ways to temperature: (1) cold temperatures increase the lubricant viscosity, and therefore increase the viscous drag torque, and (2) temperature gradients between the inner and outer race affect the loading on the balls, which can affect both runout and friction torque. In order to mitigate both of these effects, resistive strip heaters will be installed to the titanium shaft and housing parts.

Another important consideration in any successful lasercom system is stray light suppression. The optical volume of the CPA features a variety of materials and surface finishes, which, if otherwise left uncoated, would contribute significantly to scattered light reflecting back through the system. In order to limit scattering in our system, various absorptive coatings were used on all parts within the optical volume, including anodizes, ceramic coatings, filled epoxies, and paints.

3. ANALYSIS

3.1 Thermal analysis

Transient thermal analyses were performed using I-DEAS TMG to help guide the CPA thermal management design and ensure all CPA thermal requirements were met. Among the thermal design trades were selection of the exterior surface finish selection and sizing of the drive heaters. The main objectives here were to minimize temperature swings between hot and cold cases, and to minimize the amount of orbit-averaged heater power required to maintain the desired drive temperature setpoints. In the end, aluminized-Kapton Multi-Layer Insulation (MLI) blankets were selected for their high solar absorption and low radiative emissivity. Detailed design of the blankets and mounting interfaces is yet to be completed.

3.2 Structural analysis

Several rounds of structural analysis were performed throughout the design phase to guide various aspects of the system design. A detailed finite element model (FEM) was developed and matured using NX/NASTRAN, Hypermesh and FEMAP. A view of the FEM is shown below in Figure 7. The FEM has a relatively high level of detail (280,000 nodes) for a structural dynamics model. Most components were modeled with shell or brick (solid) elements. The bearings were modeled with a combination of RBE3 (interpolation) and spring elements using vendor-provided stiffnesses. FEM parameters were tuned based on a random vibration test and correlation study performed on a CPA Engineering Development Unit (EDU), as described in Section 4.2. The test showed the vendor-provided stiffnesses to be very accurate for the load levels we tested.

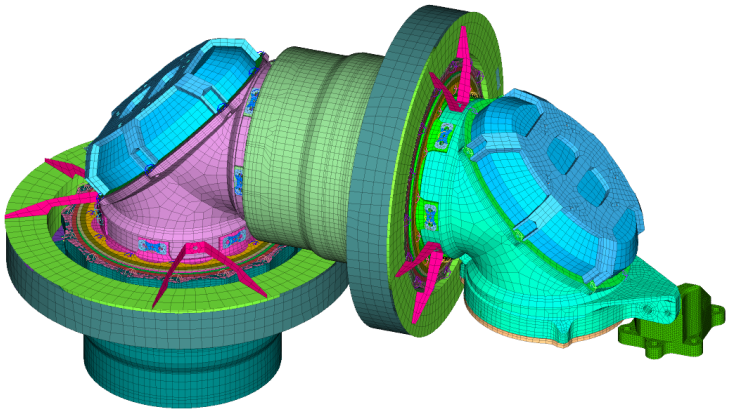

Figure 7. Structural FEM mesh

3.3 Optical analysis

Structural-thermal-optical-performance (STOP) analysis was performed on the CPA using the deployed configuration of the FEM. The STOP analysis addressed two performance environments: operational thermal and operational random vibration (jitter). Multi-point constraint (MPC) equations were built into the FEM using optical influence coefficients for the mirrors so that line-of-sight angles could be recovered in a frequency- and phase-consistent manner for jitter (as described in [26]). The same MPC equations were used to assess path angles for thermal distortion.

Jitter analysis was performed as a random frequency response analysis on the deployed CPA with 6-DoF (simultaneous, uncorrelated) translational acceleration and rotational PSD inputs. Overall RMS pointing error values were recovered

and assessed relative to allocated error budgets. Several iterations of modal optimization were performed to reduce overall pointing and path errors.

Thermally induced surface figure error of the two CPA mirrors was assessed using breakout FEMs of the mirrors, flexures, and surrounding structures. This analysis was used to optimize the titanium flexures to reduce surface figure error due to CTE mismatch between the Zerodur mirror and the aluminum support structure. The flexures were optimized for thermal distortion, modal frequency, and stress (both from random vibration and thermal distortion). RMS mirror distortions (after removing rigid-body motion) were calculated for the mirrors for max operational temperatures and compared to budgeted allowables.

4. INTEGRATION & TEST

4.1 Assembly & integration

The prototype CPA was built in stages within a clean room facility. Because of the precision demands of the final assembly, tooling was utilized at many steps in the process, including resolver and motor centration and bonding, rotor-to-stator assembly, and bearing installation and preloading. Figure 8 shows some of these assembly steps and tooling fixtures.

The precision and performance requirements of the CPA mandated a strict CMM inspection process in addition to any inspection requirements leveled on the vendors. Another notable assembly step was the match grinding of the bearing retainers, required to hard preload the duplex, angular contact bearings.

In order to achieve maximum accuracy of the resolvers, the stator and rotor components were required to be concentric within a very tight tolerance. Initially this required tightly toleranced titanium drive assemblies and the use of an air bearing to center the components, with respect to the bearing mounting features, before bonding in place. After more in-depth discussion with the resolver vendor, we learned that they often bond resolver components into mating assemblies and perform a final grind, thereby ensuring adequate concentricity without costly precision-toleranced parts and alignment stages.

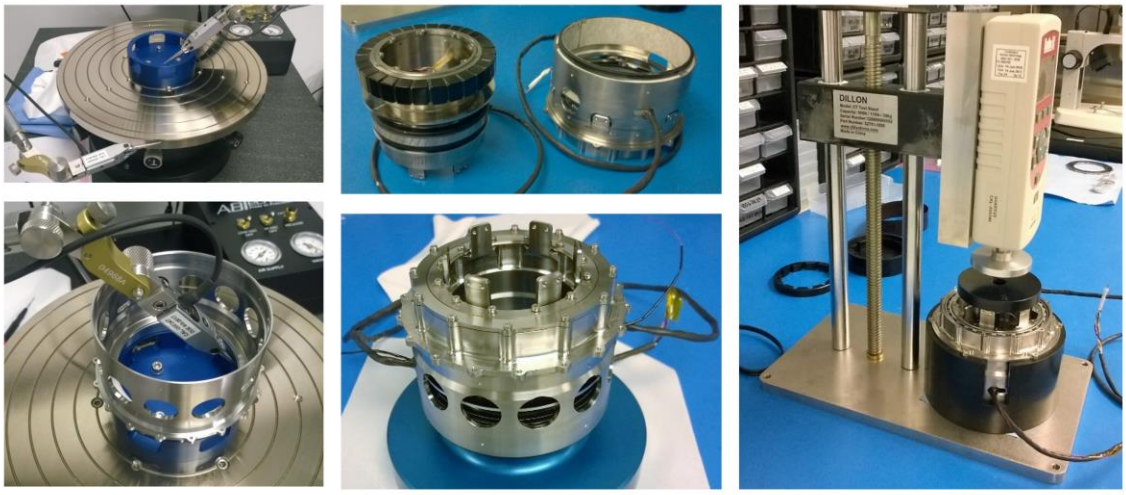

Figure 8. Various assembly steps and tooling fixtures

4.2 Vibration testing

Once the prototype CPA was assembled, it was subjected to vibration testing. There were two primary goals for this testing: verify structural integrity of system to reduce risk of hardware failure, and characterize bearing stiffness and damping, in order to improve the accuracy of future analytical models. A secondary objective was to characterize bearing friction torque before and after exposure to random vibration, in case there were significant effects due to gapping, or exceedance of smooth running allowables for Hertzian contact stress[27]. A picture of the random vibration test assembly is shown in Figure 9.

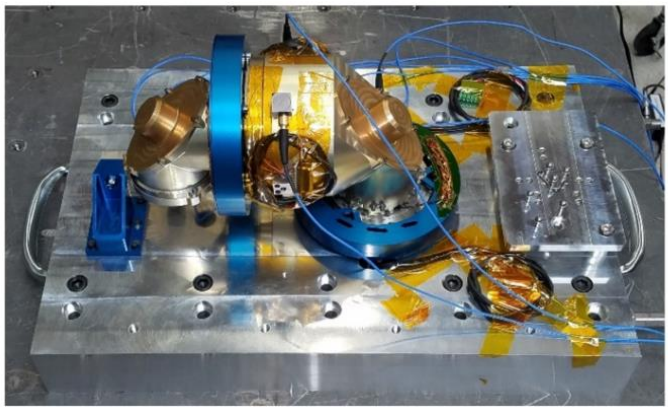

FEM vs. Test Modal Frequency Correlation

	F1	F2	F3	F4	F5
Test	137	254	436	455	568
FEM	139	251	427	469	561
%Error	1%	-1%	-2%	3%	-1%

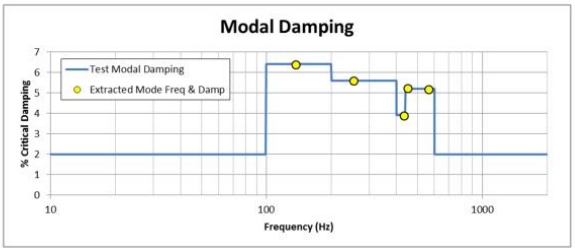

Figure 9. CPA vibration test setup & frequency / damping correlation

In each of the three axes, the unit was subjected to three vibration environments, in the following order.

1. Pre-random sine sweep (amplitude = 0.1 g, 4 octaves/min, range = 5 to 2,000 Hz, sweep both up and down)
2. Random vibration profile with increasing intensity stepping up from -12 dB to full 0 dB proto-flight level.
3. Post-random sine sweep, with the same parameters as the pre-random sweep.

The pre- and post-random sine responses were compared to determine any change in the structure due to the random environment. Vibration levels and durations are shown in Table 1.

Table 1. Random vibration test levels and durations

Frequency	-12 dB	-6 dB	-3 dB (Acceptance)	0 dB (Qual)
[Hz]	[G^2/Hz]	[G^2/Hz]	[G^2/Hz]	[G^2/Hz]
20	0.003	0.007	0.013	0.026
50	0.020	0.040	0.080	0.160
800	0.020	0.040	0.080	0.160
2000	0.003	0.007	0.013	0.026
G_{RMS}	5.0	7.1	10.0	14.1
Duration	15 sec	15 sec	15 sec	1 min

Modes extracted from the test results were used to correlate a finite element model of the CPA test assembly. As stated above, the correlation effort attempted to characterize and accurately update the model for the bearing stiffness and damping values. All model correlation was performed based on the -3dB test results, which represent “acceptance” levels, and will yield slightly lower (i.e., more conservative) damping values and more accurate response predictions for operational loads. Initial comparisons of the FEA predictions against test results indicated the FEM was capturing the dynamics of the system very well with a maximum modal frequency difference of 3% in Mode 4 (as shown in Figure 9).

LMS test management software was used to extract modal damping values from the captured frequency response functions (FRFs). The initial FEM was modeled with an assumed 2% critical damping across the entire frequency range. Extracted shapes revealed that there was much more damping in the system modes than assumed. The modal damping extracted from LMS is illustrated in Figure 9 with yellow dots indicating the damping level for each of the first five modes.

Starting from the modal differences seen in Figure 9, a correlation was performed to target actual bearing stiffness and damping values for the CPA. The correlation effort yielded two updates to the model’s damping:

- Added modal damping to the full structure slightly less than the extracted modal damping values in Figure 9.
- Increased bearing damping by adding 5% structural damping to these elements

Based on observations and measurements before, during, and after exposure to random vibration, the prototype CPA experienced no visible damage or noticeable change in mechanical performance, torque, or runout. There was, however, some indication of bearing settling with increased random vibration load level. Bearing settling was marked by a slight decrease in stiffness and increase in damping.

4.3 Torque testing

When designing the drive assemblies, we needed to ensure that the motors were able to provide adequate actuation torque to produce the intended motion of the system, despite resistance torques such as viscous friction, bearing (dry) friction, flex wrap stiffness, inertia, etc. A torque budget was established to account for all of these terms, and also to predict the required motor power required to achieve the desired motion. Safety factors were applied on top of each torque budget contributor, in accordance with the recommendations in [28]. In order to reduce risk and minimize the amount of blatant overdesign based on conservative safety factors, we also built up several bearing assemblies and measured their drag torque in various conditions. We measured different bearing diameters, different lubricants, different fill percentages, and different temperatures. We also took some measurements with and without the flex wraps installed. The test setup for this campaign consisted of a unit under test (UUT) mounted within a thermal chamber, and a reference drive motor, torque cell, and optical encoder mounted outside the thermal chamber. The UUT inside the chamber was mechanically coupled to the shaft of the reference motor and instrumentation outside the chamber. This same setup was also used later for flex wrap lifetime testing, as described in Section 4.4 and illustrated in Figure 5. An illustration of this test setup with a UUT inside the chamber is shown in Figure 10, alongside some example torque data collected with and without flex wraps.

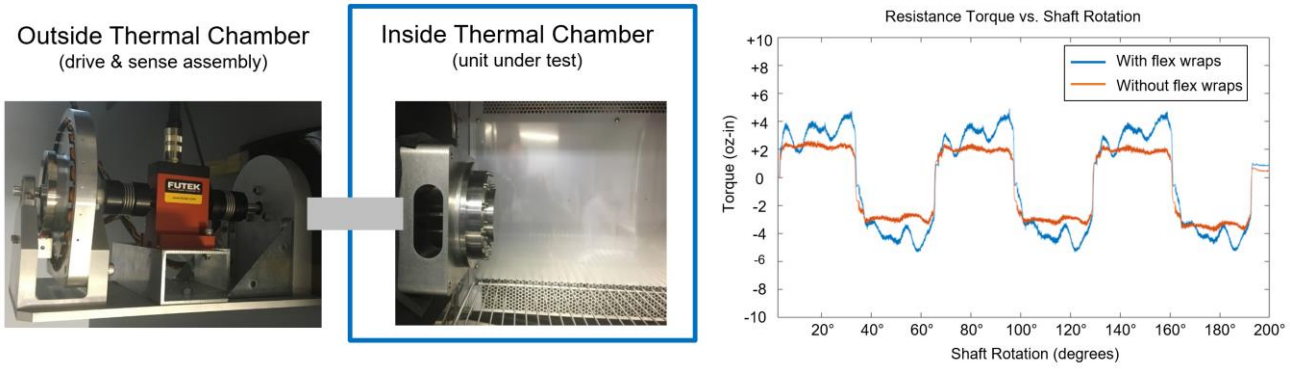

Figure 10. Drag torque measurement rig

As expected, the torque required to drive the bearing and cable wrap was very dependent on temperature, since both the lubricant viscosity and the flex wrap stiffness increased as temperatures decreased. Early test results motivated the addition of strip heaters to maintain a sufficiently warm temperature at the bearings, which thereby motivated the use of MLI blanketing to keep the CPA warm and minimize the amount of heater power required.

4.4 Flex wrap lifetime testing

The FPCs described in Section 2.5 will undergo numerous dynamic flexing cycles in operation, so lifetime testing was performed on the flex wraps to help guide detailed FPC design, and to reduce the risk of premature fatigue failure in operation. This testing involved thousands of cycles moving through the entire flex wrap range of travel, measuring resistance on each trace throughout the experiment. This testing was conducted using the same test setup that was used for torque testing, as described in Section 4.3, with the addition of a multi-channel data acquisition system to measure resistance in each FPC trace. Resistance was used to indicate onset of failure, since continuity-based methods such as those described in IPC and ASTM standards do not detect the onset of micro-cracking[29,30].

Indeed, some of our early tests produced micro-cracking failures on the copper traces, which eventually led to full "open trace" detection. These initial FPCs consisted of a dual-layer design, with one copper signal layer and one cross-hatched shield plane layer. Three different pin-count variants of this design were tested together: a 9-pin, a 15-pin, and a 21-pin FPC. The cable trays that housed the FPCs were space-limited, and the resulting bend radius of 9 mm, along with sub-optimal FPC construction, resulted in an inadequate lifetime before failure. Further testing at different temperatures indicated that this failure mode happened sooner (shorter lifetime) at higher temperatures.

As part of the failure investigation, we have explored several additional design references and obtained more extensive literature[31,32]. New lifetime calculations then drove the exploration of other FPC designs. The leading design as of this writing included reduced weight copper, increased trace width for improved crack propagation resistance, symmetric / balanced shield layers, and "book-bound" single-layer FPCs for reduced bending stress. Our latest design has been tested to over 33,000 cycles at elevated temperatures without any increase in trace resistance, and based on the sizing formula in IPC-4562, is predicted to have an infinite fatigue life.

4.5 Resolver calibration

The decision to use resolvers instead of optical encoders was primarily driven by the lack of qualification data for leading optical encoders, compared to the robustness and heritage of resolvers operating in harsh environments. Initially, it was thought that this decision would carry the consequence of significant degradation in position measurement accuracy. However, it turned out that a significant component of the resolver error is repeatable, and can therefore be calibrated out. By using a dedicated fixture, with temporarily installed optical encoders used as a "truth" sensor, we were able to calibrate the resolver against the encoder from an initial error of ± 200 µrad down to ± 20 µrad. (Note that the accuracy of the encoder itself is around 10 µrad, so there is not much point in pursuing additional calibration fit here). Sample before- and after-calibration results are shown in Figure 11, alongside a photograph of the resolver calibration fixture. Thermal cycling and then re-calibrating a drive has yielded similar calibration maps, indicating that the calibration is stable over environment, and can be trusted throughout operation.

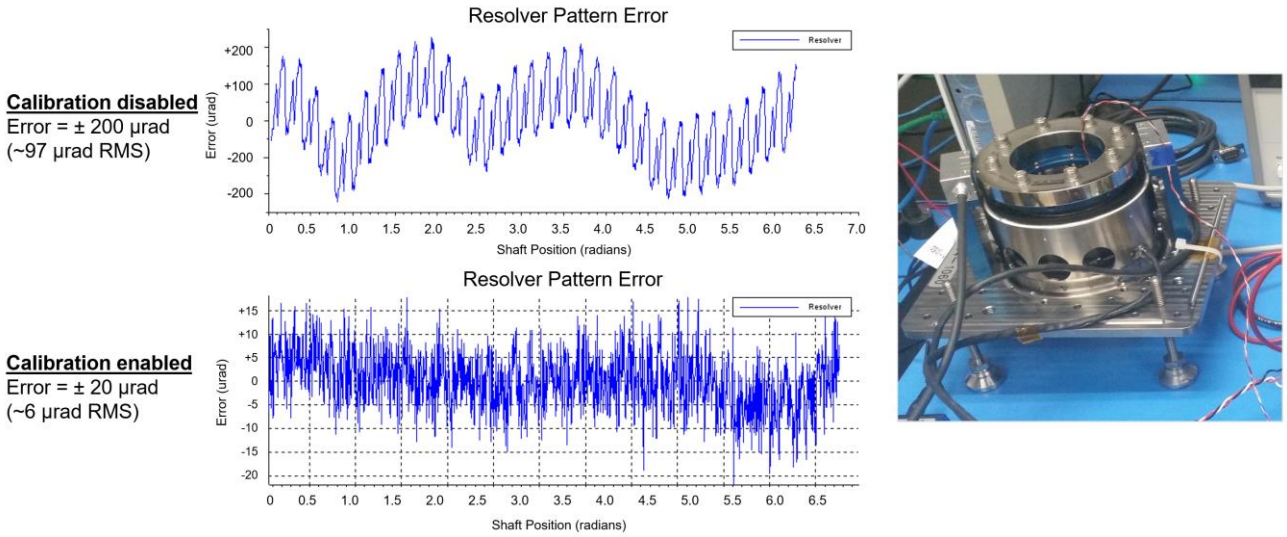

Figure 11. Resolver calibration results and fixture assembly

5. CONCLUSION

5.1 Summary

In summary, we have designed, analyzed, assembled, and tested a prototype coarse pointing assembly for laser communication. A focus on simplicity and maintaining a path to future low-cost production has manifested itself in the use of COTS components, conventional material selection (predominantly aluminum and titanium), and minimal mechanical complexity. Thermal, structural, and optical performance analyses were used to help guide various design decisions throughout the system. Various tooling fixtures were assembled and used to integrate the prototype hardware. (The final design weighs 3.8 kg and the motor power required in operation should be less than 1.0 W.) Vibration testing was conducted to verify structural integrity, and also to help adjust FEA model parameters to produce more-accurate predictions in the future. Drag torque testing was conducted to help wring-out conservatism from our torque budget, and to help motivate the need for bearing heaters. Flex wrap testing was performed to help optimize the FPC design details. Finally, the as-installed position feedback accuracy with resolvers was calibrated down to ± 20 µrad.

5.2 Future work

Based on our experience in developing this CPA design, we believe that the following topics would make for interesting research projects that could help inform future design efforts.

- Seek environmental qualification for absolute optical encoders, or other up-and-coming rotary position sensing devices. Although we were able to make resolvers work in our system, encoders would still offer slightly better accuracy, a nicer digital interface, and reduced calibration effort required.
- Perform a cost vs. performance trade for producing elbow and drive parts out of AlBeMet or other materials. Although we decided to use aluminum and titanium for this prototype, advanced materials could be used to optimize the system weight, and production at larger scale could reduce the additional cost over conventional materials to be less than the associated launch cost of a heavier system.
- Comprehensive studies on bearing drag torque and FPC fatigue lifetime as a function of the various associated design parameters could help future designers arrive more quickly at a viable design. A bearing drag torque study that produced heuristic sizing relations for direct incorporation into a torque budget would be very useful, as would a FPC lifetime study that included comparisons not just of FPC design parameters, but overall wrap arrangement (e.g., “vertical gooseneck” vs. “horizontal gooseneck” vs. “clockspring”[23]) as well.

5.3 Acknowledgements

This project was funded by the Facebook Connectivity Lab. We would also like to thank and acknowledge Brian Parris, Kyle Laudner, Bill Purdy, Eric Booen, Andrew Nichols, Janak Carey, and Nathan Woodcock for their support on this project.

REFERENCES

[1] Hemmati, H., [Near-Earth Laser Communications], CRC Press (2009).
[2] Majumdar, A., [Free-Space Laser Communications: Principles and advances], Springer (2008).
[3] Aviv, D., [Laser Space Communications], Artech House (2006).
[4] Trondle, D., et al., "Alphasat-Sentinel-1A Optical Inter-Satellite Links: Run-Up for the European Data Relay Satellite System," Proc. SPIE 9739 (2016)
[5] Boroson, D., et al., "Overview and results of the lunar laser communication demonstration," Proc. SPIE 8971 (2014).
[6] Wilson, K.E., et al., "Preliminary results of the OCTL to OICETS optical link experiment (OTOOLE)," Proc. SPIE 7587 (2010).
[7] Fields, R., et al., "NFIRE-to-TerraSAR-X laser communication results: satellite pointing, disturbances, and other attributes consistent with successful performance," Proc. SPIE 7330 (2009).
[8] Tolker-Nielsen, T., Oppenhauser, G., "In Orbit test result of an operational optical intersatellite link between ARTEMIS and SPOT4, SILEX," Proc. SPIE 4635 (2002).
[9] Tolker-Nielsen, T., et al., "In orbit test results of the first SILEX terminal," Proc. SPIE 3615 (1999).
[10] Wilson, K.E., et al., "Preliminary results of the Ground/Orbiter Lasercomm Demonstration experiment between Table Mountain and the ETS-VI satellite," Proc. SPIE 2699 (1996).
[11] "European Data Relay System: The SpaceDataHighway", ESA, https://goo.gl/yeLSCj.
[12] Rigolle, M., "LeoSat – A new satellite paradigm", SatMagazine, June 2016, https://goo.gl/CCe2cG.
[13] "Surrey Satellite and BridgeSat to Develop Free-Space Satellite Optical Communications Solution," BridgeSat, 12 April 2016, https://goo.gl/UCR27f.
[14] Mohney, D., "Making Sense of SpaceX, Boeing, and Other Mega Satellite Broadband Projects," TechZone360, 22 November 2016, https://goo.gl/K7PYfw.
[15] Dano, M., "Google teams with SpaceX for possible optical-laser powered wireless Internet service," FierceWireless, 21 Jan 2015, https://goo.gl/HGzzHS.
[16] Hempel, J., "Inside Facebook's ambitious plan to connect the whole world," Wired, 19 January 2016, https://goo.gl/qQezUy.
[17] Talmor, A., et al., "Two-axis gimbal for air-to-air and air-to-ground laser communications," Proc. SPIE 9739 (2016).
[18] Székely, G., et al., "A Coarse pointing assembly for optical communication," Proc. 40th Aerospace Mechanisms Symposium, NASA/CP-2010-216272 (2010).
[19] Chishiki, Y., et al., "Overview of optical data relay system in JAXA," Proc. SPIE 9739 (2016).
[20] Satyarthi, S., "Optical line-of-sight steering using gimbaled mirrors," Proc. SPIE 9076 (2014).
[21] Conley, P.L., [Space Vehicle Mechanisms: Elements of Successful Design], John Wiley & Sons, Inc. (1998).
[22] Vukobratovich, D., Schaefer, J.P., "Large stable aluminum optics for aerospace applications," Proc. SPIE 8125 (2011).
[23] Mäusli, P., et al., "Rotating electrical joints with continuous metallic connections," Proc. 10th ESMATS (2003).
[24] Videira, E., et al, "Design, assembly, and preloading of ball bearings for space applications - lessons learned and guidelines for success," Proc. 15th European Space Mechanisms & Tribology Symposium, Vol. 718 (2013).
[25] Jones, J.R. Jr. and Jansen, M.J., "Space Tribology," NASA/TM-2000-209924 (2000).
[26] Doyle, K., et al., [Integrated Optomechanical Analysis], SPIE Press (2012).
[27] "Design and Development Requirements for Mechanisms," NASA-STD-5017A (2016).
[28] "General Environmental Verification Standard," NASA GSFC-STD-7000A (2013).
[29] Beck, D.F., et al, "Fatigue behavior of thin Cu foils and Cu/Kapton flexible circuits," Sandia National Laboratories, SAND2008-4293C (2008).
[30] Oshida, Y., and Chen, P.C., "Nondestructive low-cycle fatigue characterization of multi-layer thin film structures," *Journal of Nondestructive Evaluation*, 8(4), 235-245 (1989).
[31] Beck, D.F., "Assessing the operational life of flexible printed boards intended for continuous flexing applications -- a case study," Sandia National Laboratories, SAND2011-0564 (2011).
[32] Martynenko, E., et al, "High cycle fatigue resistance and reliability assessment of flexible printed circuitry," Journal of Electronic Packaging, 124(3), 254-259 (2002).